



Geology of late-Variscan Sàrrabus pluton (south-eastern Sardinia, Italy)

F. Secchi, S. Naitza, G. Oggiano, S. Cuccuru, A. Puccini, A. M. Conte, T. Giovanardi & M. Mazzucchelli

To cite this article: F. Secchi, S. Naitza, G. Oggiano, S. Cuccuru, A. Puccini, A. M. Conte, T. Giovanardi & M. Mazzucchelli (2021) Geology of late-Variscan Sàrrabus pluton (south-eastern Sardinia, Italy), Journal of Maps, 17:2, 591-606, DOI: [10.1080/17445647.2021.1982032](https://doi.org/10.1080/17445647.2021.1982032)

To link to this article: <https://doi.org/10.1080/17445647.2021.1982032>



© 2021 The Author(s). Published by Informa UK Limited, trading as Taylor & Francis Group.



[View supplementary material](#)



Published online: 31 Dec 2021.



[Submit your article to this journal](#)



Article views: 506



[View related articles](#)



[View Crossmark data](#)



Geology of late-Variscan Sàrrabus pluton (south-eastern Sardinia, Italy)

F. Secchi ^{a,c}, S. Naitza ^{b,c}, G. Oggiano ^a, S. Cuccuru ^a, A. Puccini^a, A. M. Conte^d, T. Giovanardi^e and M. Mazzucchelli^e

^aDipartimento Chimica e Farmacia, Università degli Studi di Sassari, Sassari, Italy; ^bDipartimento Scienze Chimiche e Geologiche, Cittadella Universitaria Monserrato (CA), Università degli Studi di Cagliari, Cagliari, Italy; ^cCNR-Istituto di Geologia Ambientale e Geoingegneria, Sede Secondaria di Cagliari, Cagliari, Italy; ^dCNR-IGAG, Sede di Roma, c/o DST Sapienza Università di Roma, Roma, Italy; ^eDipartimento Scienze Chimiche e Geologiche, Università degli Studi di Modena e Reggio Emilia, Modena, Italy

ABSTRACT

This paper deals with the geological mapping of the late-Variscan Sàrrabus pluton, (south-eastern Sardinia), a shallow multiple and composite igneous complex dominated by several generations of granodiorites, metaluminous and peraluminous granites and repeated pulses of mantle-derived mafic magmas. The map has been compiled based on geological surveys at 1:10,000 and 1:5,000 scales, assisted by *in situ* gamma-ray spectrometry and detailed petrographic investigations. Granite-related ore deposits have been also reported. The emplacement age of the pluton can be constrained by U/Pb dating on zircons of Cala Regina granodiorite, yielding an age of 286 ± 9 Ma. The resulting scenario documents a bimodal magmatism controlled by an EW trending shear zone, followed by the shallower emplacement of several pulses of independent granite magmas.

ARTICLE HISTORY

Received 25 February 2021
Revised 10 August 2021
Accepted 23 August 2021

KEYWORDS

Late-Variscan magmatism; gamma-ray logging; shear zone; bimodal magmatism

1. Introduction

The Sardinia-Corsica block is a segment of the Southern Variscan Belt (Carmignani et al., 1994; Rossi et al., 2009), resulting from the early Carboniferous collision between Laurussia and Gondwana (Matte, 1986). In detail, the Variscan collisional frame of Sardinia and Corsica results in a high-grade, inner, anatectic complex retaining remnants of eclogite and HP mafic granulite (Corsica and northern Sardinia; Cruciani et al., 2015, 2020), which overthrusts a pile of nappes showing low- to medium-grade metamorphism. The nappes in turn override with overall top- to- southwest transport a non-metamorphic foreland exposed in southern Sardinia (Carmignani et al., 1994). In late Carboniferous-early Permian (Cocherie et al., 2005), the metamorphic basement was intruded by a wide compositional spectrum of post-collisional coalescent plutons commonly showing a high-K calcalkaline affinity, forming the Sardinia-Corsica batholith (Bonin, 2004; Casini, Cuccuru, Puccini, 2015; Cocherie et al., 2005; Conte et al., 2017; Edel et al., 2014; Ferré & Leake, 2001; Paquette et al., 2003; Rossi et al., 2015; Rossi & Cocherie, 1991).

According to Conte et al. (2017), the southern part of the Sardinia batholith grew during two main magmatic peaks (Naitza et al., 2015), clustered around 305 Ma (Old Magmatic Peak, OMP) and 285 Ma (Young Magmatic Peak, YMP). A complex succession of

tectonic and magmatic events marks these two stages of batholith growth and, at present, no single and generally accepted model exists to account petrogenesis and spatial/chronological relationships among its intrusive sequences.

Plutons emplaced within different tectono-metamorphic portions of the Sardinian basement show different geological features in terms of emplacement style and mantle/crust contribution. In the axial zone (N Sardinia), pre-300 Ma calcalkaline plutons are dominated by monzogranites; between 300 and 285 Ma, granodiorite volume increases. Conversely, the pre-300 Ma intrusives occurring in the Nappe Zone are dominated by granodiorites, while leucogranites represent the younger intrusions (Conte et al., 2017, and references therein).

Recent papers emphasized the control of lithospheric shear zones on the emplacement of major plutons outcropping in northern Sardinia (Casini et al., 2012; Casini, Cuccuru, Maino, et al., 2015; Casini, Cuccuru, Puccini, 2015; Cuccuru et al., 2018; Edel et al., 2014), and the involvement of meta-igneous and meta-pelitic crustal sources with subordinate mantle contribution (Bralia et al., 1982; Cocherie et al., 1994; Conte et al., 2017; Di Vincenzo et al., 1996, 1999; Poli et al., 1989; Rossi et al., 2015; Tommasini et al., 1995). When referred to Frost and Frost (2011) petrochemical discrimination diagrams, the

CONTACT S. Naitza snaitza@unica.it Dipartimento Scienze Chimiche e Geologiche, Cittadella Universitaria Monserrato (CA), Università degli Studi di Cagliari, S. S. 554 bivio per Sestu, I-09042 Cagliari, Italy; CNR-Istituto di Geologia Ambientale e Geoingegneria, Sede Secondaria di Cagliari, Via Marengo 2, 09123 Cagliari, Italy

© 2021 The Author(s). Published by Informa UK Limited, trading as Taylor & Francis Group.

This is an Open Access article distributed under the terms of the Creative Commons Attribution License (<http://creativecommons.org/licenses/by/4.0/>), which permits unrestricted use, distribution, and reproduction in any medium, provided the original work is properly cited.

compositional shift from production of prevalingly *magnesian* magmas to *ferroan*, crustal-derived F-bearing magmas, marks the transition between the OMP and YMP. Overall, large areas of the batholith lack detailed geological and structural field mapping, along with dating on the single intrusions. In addition, mafic and acidic dike swarms spread at regional scale are still awaiting to be framed in the different pre-, syn- and post-magmatic stages of batholith growth.

This paper deals with the Sàrrabus igneous massif, which is a wide (400 km²) multiple and composite pluton located in south-easternmost part of the batholith. It shows a complex architecture, including uncommon suites (i.e. hastingsite granites) and, compared to other massifs at the scale of the Variscan belt, a large incidence of mafic dikes. Previous studies (Conte, Cucuru, et al., 2018; Conte et al., 2017; Conte, Naitza, et al., 2018; Poli & Tommasini, 1999; Ronca et al., 1999; Secchi & Lorrain, 2001) evidenced petrogenetic processes involving repeated production of felsic magmas from meta-igneous sources at different crustal levels, and production of mantle-derived magmas. A wide network of fluorite-barite and Pb–Ag sulfide hydrothermal veins, mostly hosted in the metamorphic basement close to the contact with the intrusives is also spatially and genetically associated with the Sàrrabus pluton.

Within this scenario, the geological map represents a mandatory basic tool for disclosing the tectono-magmatic history of the massif. In this regard, some unsolved issues mainly concern the discrimination within different intrusive units of similar composition and internal petrographic and structural features. Mapping ⁴⁰K, ²³²Th and ²³⁸U abundances through a portable, high-sensitive gamma-ray spectrometer have been successful in discriminating granite pulses in northern Sardinia (Kaçeli Xhixha et al., 2016; Puccini et al., 2014) and was employed to improve the map detail. The geostatistical processing of more than 100 in situ measurements better allowed the distinction among units and was useful in the reconstruction of the architecture of the Sàrrabus igneous massif, providing a geological-structural map at 1:50,000 full scale realized with a multi-methodological approach.

2. Methods

2.1. Petrographic studies

Geological field surveys were coupled with a detailed petrographic study on more than 500 thin sections.

2.2. Remote sensing

A Digital Elevation Model (DEM) was created from a mosaic of 1:10,000 topographic maps. The DEM was integrated with geo-referenced high-resolution aerial

orthophotos (property of Regione Autonoma della Sardegna) and IKONOS 2005 (Regione Autonoma Sardegna, 2005) satellite images. Detailed information about correlated errors, spatial resolution and image accuracy, are reported in Viridis et al. (2012). Results were processed to boost geomorphological features related to dikes, major faults, joints networks, and lithological contacts within the composite pluton, deduced by different fracture patterns as well as different weathering styles. Data were finally processed in GIS environment, overlaid and integrated with geological data and converted into digital maps.

2.3. Structural data

Magmatic flow-trajectories in granodiorites were deduced by the preferred orientation of microgranular dark enclaves, feldspar megacrysts in the inequigranular facies as well as aplo-pegmatitic veins, stretching lineation was deduced by major axis of enclaves and K-feldspar orientation. Poles to foliation were projected in conventional stereoplots to document the statistical distribution of magmatic foliation and to constrain the resulting geometry of the pluton and the evolution of emplacement mechanisms for various intrusive units.

2.4. Gamma-ray spectrometry

The occurrence of different coalescing intrusions in the narrow monzogranite-leucogranite compositional range, and the abundance of colluvium covers and regolith required an improvement of geological surveys by in situ gamma ray. Specific activities of ⁴⁰K, ²³⁸U and ²³²Th were measured using a portable gamma-ray spectrometer equipped with a 1-liter NaI (Tl) scintillator, in more than 100 representative outcrops (Table 1) of magmatic and surrounding metamorphic rocks, according to the procedure reported in Puccini et al. (2014) and Kaçeli Xhixha et al. (2016). The uncertainty of the method is estimated to be 1.5%, 3% and 3% for ⁴⁰K, ²³⁸U and ²³²Th, respectively (Caciolli et al., 2012). Data were interpolated in GIS environment with the Inverse Distance Weighting algorithm in order to realize three radionuclide maps.

2.5. Geochronology

A representative sample of Cala Regina Unit granodiorite from Capo Carbonara area was selected for in situ U/Pb zircon dating to compare U/Pb ages with previously published chronological data obtained in the same locality by K/Ar and Rb/Sr internal isochrones by Nicoletti et al. (1982).

Zircons were analyzed both by 100-µm thin section thick or extracted from 3 to 4 kg of sample using

Table 1. ^{232}Th , ^{238}U and ^{40}K average data for Sàrrabus igneous massif σ refers to standard deviation; b. d. l. = data below detection limit. Data collected for metamorphic basement are reported for comparison.

Mapped rock unit	Measurements	Th^{232} (ppm)-				U^{238} (ppm)				K^{40} (weight %)			
		Mean	Min	Max	$\pm\sigma$	Mean	Min	Max	$\pm\sigma$	Mean	Min	Max	$\pm\sigma$
<i>Burcei</i> (BU)	2	12.02	11.38	12.67	0.91	2.69	2.67	2.71	0.03	2.54	2.33	2.76	0.30
<i>Monte Cresia</i> (MC)	5	18.06	13.84	21.75	3.63	4.89	3.90	5.84	0.90	3.53	3.20	3.78	0.24
<i>Monte Nai</i> (MN)	20	17.17	12.27	24.01	3.18	5.28	2.80	8.88	1.49	3.83	3.16	5.04	0.53
<i>Cala Regina</i> (CR)													
Granodiorites	26	15.31	8.42	26.15	3.83	3.81	1.51	6.74	1.11	3.42	1.99	6.21	0.94
Gabbrotonalites (SO)	6	3.46	1.50	6.91	2.11	1.09	0.30	2.41	0.84	0.81	b.d.l.	2.07	0.92
Epsienites (S)	7	10.31	5.00	16.89	4.06	3.23	1.60	5.40	1.30	0.55	b.d.l.	2.85	1.08
<i>Brunco Nicola Bove</i> (BNB)	17	16.66	13.47	20.58	1.92	4.78	3.20	10.00	1.47	3.81	2.96	4.62	0.42
<i>San Priamo</i> (SP)	20	28.15	20.30	40.32	5.77	6.65	3.74	10.29	1.97	4.66	3.76	5.69	0.56
<i>Monte Sette Fratelli</i> (SF)	8	20.59	17.83	25.19	2.67	5.18	3.29	6.57	1.05	4.36	3.68	5.43	0.63
<i>Monte Maria</i> (MM)	3	20.80	16.30	28.01	6.31	6.29	4.59	8.51	2.01	4.01	3.60	4.44	0.42
<i>Metamorphic basement</i>	3	13.07	10.01	15.50	2.78	4.30	2.77	5.99	1.61	2.81	2.26	3.62	0.71

conventional separation techniques. Final hand-picked crystals were mounted in epoxy resin and examined with cathodoluminescence imaging using a Nova Nano SEM 450 SEMFEG equipped with a CLD KE stand-alone Centaurus detector. U/Pb isotopes were determined using a quadrupole ICP-MS X Series II (Thermo Fisher Scientific) coupled to a 213 nm Nd:YAG laser ablation system (New Wave Research™) at the laboratories of the Centro Interdipartimentale Grandi Strumenti of the Università di Modena e Reggio Emilia following the analytical protocol and data processing by Giovanardi et al. (2018). U–Pb ratios were corrected for laser-induced elemental fractionation using zircon reference material TEMORA-2 (average $^{206}\text{Pb}/^{238}\text{U}$ of 0.66719 ± 0.00348 for $n = 12$; literature accepted value of 0.66710).

U/Pb obtained data have been compared to a Rb/Sr isochron obtained for selected granodiorite samples from Cala Regina Unit. Sr isotopic compositions were carried out at IGAG-CNR laboratories of University of Rome ‘La Sapienza’ (Rome, Italy) using a FINNIGAN MAT 262RPQ multi-collector mass spectrometer with W single and Re double filaments in static mode. Rb and Sr elemental concentrations were determined at Activation Laboratories, Ancaster, Ontario, Canada by ICP-MS techniques with accuracy of $\pm 5\%$.

3. Anatomy of Sàrrabus pluton

3.1. Field relationships

Eight intrusive units were recognized (Figure 1); from older to younger, the emplacement succession is reported as follows, reconstructed on the basis of common geological indicators (intersections, roof pendants, chilled margins, inclusion trains):

Burcèi Unit (gabbrotonalites; BU) → Monte Cresia Unit (granodiorites grading to monzogranites; MC) + Monte Nai Unit (granodiorites grading to monzogranites; MN) → Cala Regina Unit (granodiorites; CR) → Monte Maria Unit (peraluminous leucogranites +

Brunco Nicola Bove Unit (monzogranites grading to leucogranites; BNB) → San Priamo Unit (leucogranites; SP) → Monte Sette Fratelli Unit (monzogranites grading to leucogranites; SF).

Figure 2 documents some outcrop features and relevant emplacement relationships recognized in the field, as the Monte Maria/Cala Regina intrusive contact (Figure 2(a)) and the close mafic/felsic implication in the Cala Regina Unit.

Figure 3 displays the sharp macroscopic textural variations of mapped rock-units. Moreover, the whole data set of macroscopic features and petrographic data of mapped rock-units is summarized in Table 2.

In the following, the architecture of the pluton and the relationships between the mapped rock-units will be discussed first. Schematically, the pluton is made up of granodiorites (Cala Regina, Monte Nai and Monte Cresia Units) intruded by EW trending monzogranites and leucogranites (Brunco Nicola Bove and San Priamo Units) with a granodiorite/granite 1/1 field ratio; Monte Cresia and S. Priamo Units are in turn intruded by Monte Sette Fratelli Unit granite, which represents the last intrusive event (Figure 4).

Looking at the granodiorites, the Monte Cresia Unit outcrops discontinuously at the northern edge of the pluton, with flat contacts with the basement. It outcrops southward as a continuous belt over the Brunco Nicola Bove Unit. The Monte Cresia/Cala Regina Units relationships are less visible, but the local occurrence in the Cala Regina Unit of chilled margins is an evidence of its later emplacement. The Monte Nai Unit does not show univocal emplacement relationships with the Monte Cresia/Cala Regina Units, making it difficult to establish their intrusion sequence. Overall, the granodioritic units display definite heterogeneities in geological style and petrographic features (Table 2), further confirmed by gamma-Ray measurements (Table 1). The Cala Regina Unit granodiorites exhibit a general flat trend evidenced both by magmatic foliation and by pronounced internal grain size variations, from medium-grained foliated rocks with a high incidence of flattened dark enclaves, to fine-grained porphyritic

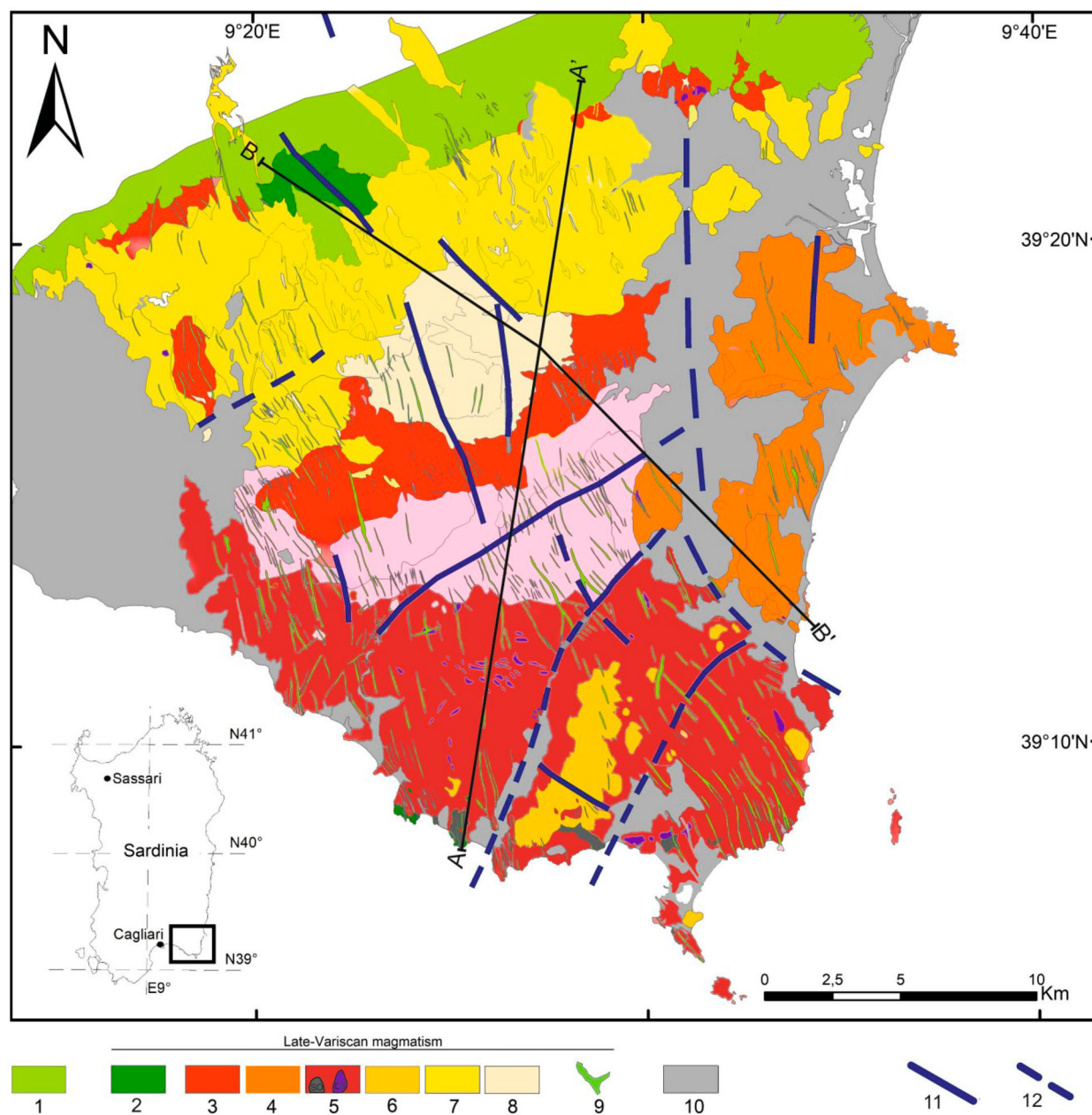


Figure 1. Geological sketch map of late-Variscan Sàrrabus pluton. (1) Undifferentiated anchimetamorphic complex (Cambrian-early Carboniferous). (2-10) Late-Variscan igneous units of Sàrrabus pluton: (2) Burcèi Unit. (3) Monte Cresia Unit. (4) Monte Nai Unit. (5) Cala Regina Unit with synplutonic mafic bodies (SO) and Na-metasomatized varieties (ES). (6) Monte Maria Unit. (7) Bruncu Nicola Bove Unit. (8) San Priamo Unit. (9) Monte Sette Fratelli Unit. (10) Mafic and acidic dikes. (11) Post-Mesozoic sedimentary and volcanic covers and recent continental and transitional sedimentary deposits (Pleistocene–Olocene). Other symbols (11-12). Main extensional faults (11), and inferred/buried faults (12). SSSZ refer to late-Variscan southern Sàrrabus shear zone. A–A' and B–B' refer to the location of cross-sections reported in Figure 4.

facies with pegmatitic pods indicating the top of the intrusion, further defined by small roof pendants of hornfelsed siliciclastic rocks. K-feldspar megacrysts granodiorites prevail in the south-eastern sector. Conversely, the Monte Cresia Unit commonly displays homogeneous equigranular textures, with rare and rounded dark enclaves. The Monte Nai Unit shows textural and compositional internal variations, ranging from granodiorite to monzo- and leucogranite. Except for Burcèi gabbrotonalites which based on geochronological constraints (see below) predates the

growth of the pluton, mafic intrusions consist of stretched and dismembered synplutonic dikes and stocks of gabbroic rocks (Solànas complex in the map; SO) that crop out for more than 10 km along a narrow EW mingled belt within the Cala Regina granodiorite (Conte et al., Conte, Naitza, et al., 2018; Secchi & Lorrain, 2001; Figure 2(b,c)). Na-rich fluid flows conveyed along this belt favored metasomatic effects in the cooling granodiorite, locally producing Na-metasomatized episyenitic rocks (S in the map) occurring as homogeneous, small, isolated bodies. Episyenites



Figure 2. Geological aspects of Sàrrabus intrusives (a) Contact field relationships between the synplutonic gabbroic body of (SO) and the crosscutting garnet-bearing leucogranites of Monte Maria unit (MM) (Scala Carbonara, eastward of Capo Boi); (b) dismembered swarm of synplutonic mafic dikes of quartz gabbroic composition within hornblende biotite granodiorites of Cala Regina unit (western slope of Torre de su Fenugu). Evidence of syn-magmatic extensional tectonics on CR Unit; (c) down-dip foliation on quartz-dioritic varieties evidenced by strongly elongated quartz gabbroic dark enclaves (Porto Murrone, west of Solànas; vertical slope); (d) down-dip foliation on granodioritic varieties evidenced by elongated quartz gabbroic dark enclaves and large feldspars (Cabu Oi west of Solànas; vertical slope); (e) evidence of different generation of dike swarms. Contact relationships between different dike generations hosted in the Cala Regina Unit: peraluminous NE trending acidic dikes (dotted lines), are displaced by NNW metaluminous acidic dikes (Cala Regina).

also form roughly layered bodies at the top of the Cala Regina intrusion and are present, more locally, in the Monte Cresia Unit.

Distinct generations of satellite intrusions occur in different settings within the pluton. True peraluminous varieties are represented by the Monte Maria Unit

garnet-bearing granite, an NNE trending stock which intrudes the Cala Regina granodiorites, and by minor bodies of two-mica fine-grained granites, intruded into a mingled zone of Cala Regina unit. The Monte Cresia/San Priamo Unit contact is exploited by the

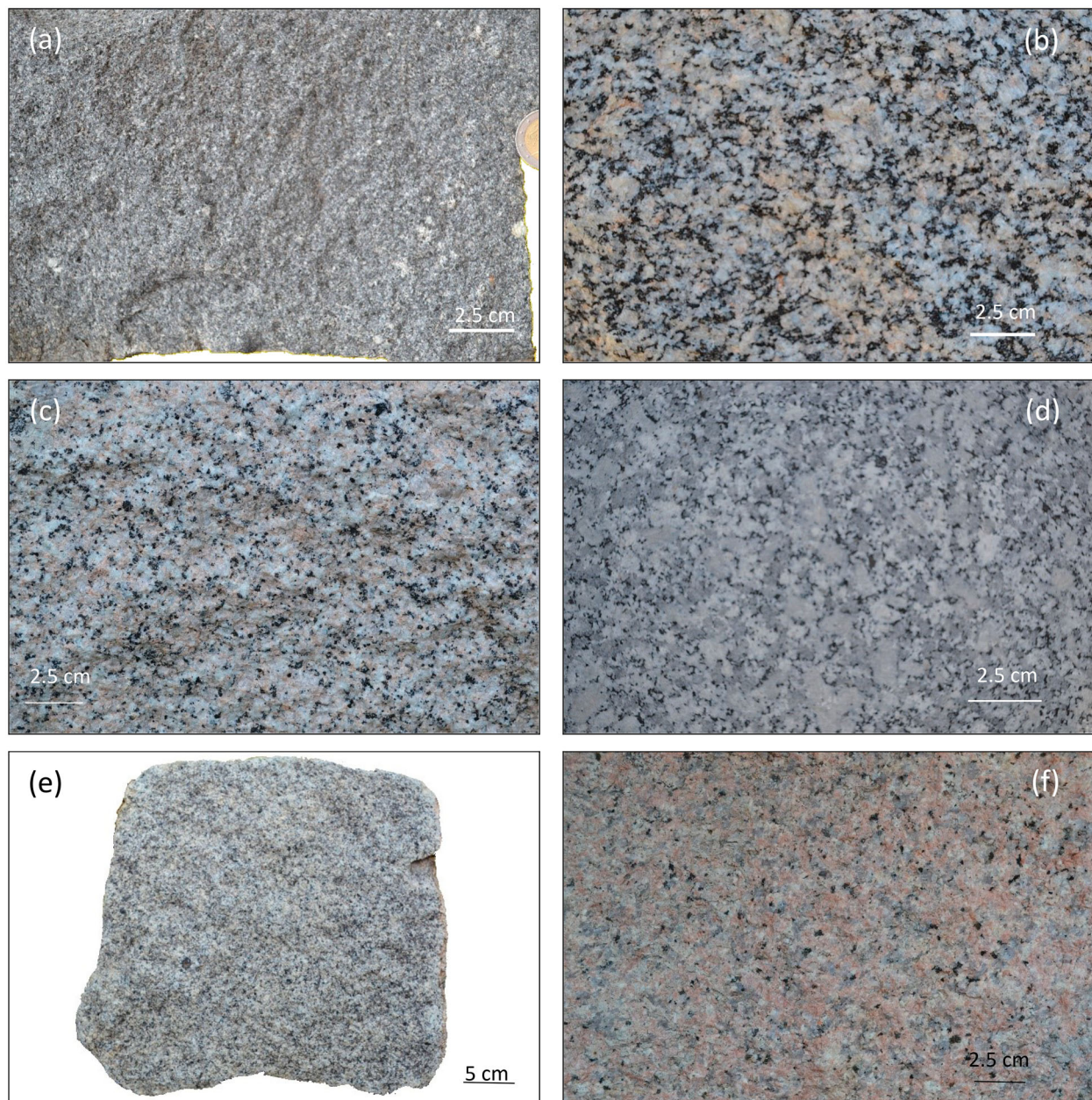


Figure 3. Macroscopic textural features of some representative rocks from Sàrrabus pluton (a) gabbrotonalite (BU Unit); (b) hornblende biotite granodiorite (Cala Regina Unit); (c) biotite granodiorite (Monte Cresia Unit); (d) inequigranular granodiorite (Monte Nai Unit); (e) hastingite granite (Monte Sette Fratelli Unit); (f) pinkish biotite granite (San Priamo Unit).

metaluminous granites of Monte Sette Fratelli Unit, emplaced as a large sub-vertical stock.

The whole pluton is crosscut by several generations of late mafic and felsic dikes. According to Conte et al. (2017) the incidence and thickness of mafic varieties strongly decrease from granodiorites to leucogranites. Felsic dikes include earlier NE trending peraluminous garnet-bearing two-micas granites (Figure 2(d)) crosscut by NNW trending mafic dikes (mostly spessartites), frequently associated with metaluminous microgranite dikes. Remarkably, the latest intrusive units (San Priamo and Sette Fratelli) are crosscut by olivine-bearing plagiophyric dikes ('tholeiitic dolerites', in Ronca et al., 1999). Finally, NNW trending granophyres and rhyolitic dikes and stocks crosscut the whole pluton

from Punta Molentis to Burcei and represent the end of Variscan magmatism in the region.

3.2. ^{40}K , ^{238}U and ^{232}Th abundances

Th/U plot (Figure 5) highlights the radiological aspects of the mapped units. The lowest radioactivity values are recorded in Burcei Unit gabbrotonalites and in the hybrid rocks shells around the synplutonic mafic bodies of the SO complex associated to Cala Regina Unit. Higher values are, conversely, typical of granitic varieties belonging to the late felsic intrusions (i.e. San Priamo and Sette Fratelli units). Coherently, collected data reported in Table 1 and plotted in the density maps (Figure 6) confirm the granites/

Table 2. Summary of geological and petrographic features of late-Variscan intrusives from Sàrrabus igneous massif (south-eastern Sardinia, Italy). Ages in are expressed in Ma.

Ages	Mapped rock-Units/serial affinity	Field and macroscopic features	Rock-textures	Mineral assemblage		
				Fundamental phases	Accessory phases	Late stage
293 ± 3	<i>Mafic dikes/(tholeiitic)</i>	Sub-vertical dikes of porphyritic olivine-bearing rocks; often strongly altered	Porphyritic	Ol + Pl → Cpx + Pl ± Hb	Ti-Mt + Ilm + Sulf + Ap	
	<i>Mafic and felsic composite dikes/calcalcaline</i>	Sub-vertical dikes mainly of spessartite composition; often strongly altered Peraluminous and metaluminous felsic dikes dominantly microgranular to aphyric	Porphyritic to hypidiomorphic and sub-ophitic textures in mafic varieties Microgranular to granophyric Microgranular to porphyritic	Pl + Hb + Qz ± Bt or: Pl + Cpx ± Ol Qz + Kfs + Pl + Bt ± Mscv ± And Qz + Kfs + Pl + Bt	Ti-Mt + Ilm + Sulf + Ap Ilm + Zrn + Ap Zrn + Ap	Turm Fl
	<i>SF Monzogranites to leucogranites (Monte Sette Fratelli unit)/ferroan</i>	Sub-vertical stock of medium to fine-grained equigranular gray-greenish rocks	Hypidiomorphic	Qz + Kfs + Pl + Hs + Ann	Aln + Mt + Zrn + Ap	Fl + Ann
	<i>SP Leucogranites (San Priamo Unit)/ferroan</i>	Equigranular pinkish coarse-grained rocks; pegmatites and quartz-fluorite at the top of intrusion. Filter-pressing sub-vertical reddish, hololeucocratic porphyries and aplites are densely intruded in the western sector	Hypidiomorphic	Qz + Kfs + Pl + Bt	Aln + Mt + Zrn	Ann + Fe-Chl
	<i>BNB Monzogranites to leucogranites (Brunco Nicola Bove Unit)/magnesian</i>	Homogeneous, grayish, medium-grained monzogranitic rocks intruded by synplutonic injections of leucogranites in stocks or E trending large dikes	Hypidiomorphic	Qz + Kfs + Pl + Bt	Ilm + Ap + Zr	
	<i>MM Peraluminous leucogranites (Monte Maria Unit)/ferroan</i>	Sub-vertical large stock and dikes of equigranular to porphyritic medium to fine-grained rocks	Hypidiomorphic	Qz + Kfs + Pl + Bt + Gt + Mscv	Ilm + Zrn + Ap	Turm
	<i>MN Granodiorites to monzogranites (Monte Nai Unit)/magnesian</i>	Medium-coarse-grained inequigranular granodiorites with few and sub-rounded dark enclaves, grading to monzogranites with fine-grained equigranular leucogranites at the top. Middledly foliated granodiorites in the eastern side of the intrusion	Hypidiomorphic	Pl + Kfs + Qz + Bt	Ilm + Ap + Aln + Mon	
286 ± 9/292 ± 17	<i>SO complex gabbrotonalites associated to Cala Regina Unit/magnesian</i>	Synplutonic mafic dikes occurring within Cala Regina granodiorites along narrow WNW shear zones. Mostly fine-grained gabbroic rocks, densely mingled with strongly foliated quartz-diorites/tonalites, grading to hornblende granodiorites. Local small olivine-bearing cumulophyric stratified bodies and pegmatitic pockets	Hypidiomorphic Panhydiomorphic/ Hypidiomorphic Cumulophyric rock-textures	Hbl + Pl + Bt + Qz ± Opx ± Cpx Pl + Hbl + Bt + Qz ± Kfs ± Opx Ol + Opx + Cpx + Pl + Qz	Tit + Mt + Ap + Ilm Ilm + Tit + Al + Zrn Mt + Ap	Actin + Cum Actin
	<i>CR Granodiorites (Cala Regina Unit)/magnesian</i>	Weakly to middly foliated medium-coarse-grained equigranular to strongly inequigranular rocks. Size, incidence and aspect ratio of dark enclaves increases southward. Na-metasomatized varieties (294)	Hypidiomorphic Automorphic to porphyritic	Pl + Kfs + Qz + Hbl + Bt Alb + Kfs + Cpx + Hs ± Bt ± Gt	Ilm + Ap + Aln + Mon ± Tit Tit + Mt + Zrn + Ap	Turm

(Continued)

Table 2. Continued.

Ages	Mapped rock-Units/serial affinity	Field and macroscopic features	Rock-textures	Mineral assemblage		
				Fundamental phases	Accessory phases	Late stage
	<i>MC Granodiorites to monzogranites (Monte Cresia Unit)/magnesian</i>	± 9 Ma) are observed along narrow WNW shear zones (S) Weakly foliated, grayish coarse- to medium-grained rocks grading upward to porphyritic monzogranites with sub-rounded dark enclaves. Sub-horizontal pegmatite veins at the top of intrusion. Na-metasomatized varieties are observed (S)	Hypidiomorphic Automorphic to porphyritic	Qz + Kfs + Pl + Bt \pm Hbl Alb + Kfs + Cpx + Hs \pm Bt	Ilm + Zrn + Ap 8 Tit + Mt + Zrn + Ap	Turm
311 \pm 9	<i>BU Gabbrotonalites (Burcei Unit)/magnesian</i>	Sub-horizontal sill. Homogeneous, equigranular to porphyritic mesocratic medium to fine-grained rocks. Widely altered, they display local thermometamorphic effects due to SP leucogranite intrusion	Hypidiomorphic to porphyritic with graphic groundmasses and cumulo-phyric norites	Pl + Qz + Kfs + Bt + Opx + Cpx	Ilm + Ap + Zrn + Sulf	Actin+Cumm

Value in boldface refer to U/Pb on zircon (Capo Carbonara); other values refer to published Rb/Sr regression lines available on Brotzu et al. (1993) for Burcei unit, Pirinu et al. (1996) for Na-metasomatized varieties, Ronca et al. (1999) for white micas from peraluminous felsic dikes and Conte et al. (2017) (San Priamo leucogranites). Abbreviations list according to Kretz (1983) and Whitney and Evans (2010): Pl = plagioclase; Qz = quartz; Kfs = K-feldspar; Bt = dark mica; Hbl = hornblende; Opx = orthopyroxene; Cpx = clinopyroxene; Hs = hastingsite; Gt = garnet; Mscv = white mica; And = andalusite; Ol = olivine; Ilm = ilmenite; Ap = apatite; Mon = monazite; Aln = allanite; Zrn = zircon; Sulph = sulphides; Mt = magnetite; Alb = albite; Fl = fluorite; Ann = annite; Actin = actinolite; Cumm = cummingtonite. Ortho and clinopyroxene observed in BU, SO rocks and mafic dikes show commonly a Hypersthene and augitic composition, respectively; they are often replaced by Actinolite and Cummingtonite. Clinopyroxene and garnet from Na-metasomatized varieties show a diopsidic and andraditic composition, respectively. Ferroan/magnesian serial character refer to Frost et al. (2001) discrimination scheme, based on chemical analyses reported in Brotzu et al. (1993) and Conte et al. (2017). Hastingsite, diopside, andradite, annite, cummingtonite and actinolite according to EMPA analyses reported in Brotzu et al. (1993), Pirinu et al. (1996), and Conte et al. (2017).

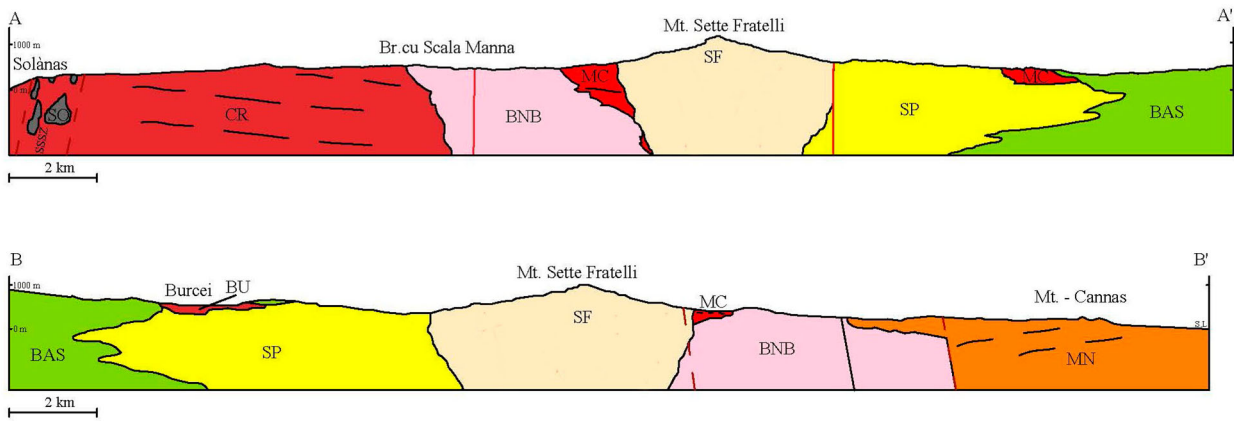


Figure 4. Schematic cross-sections for Sàrrabus pluton, as reported in Figure 3. S.L. refers to sea level; no vertical exaggeration. To simplify, dike swarms and episyenites were not plotted. BAS, BU, MC, MN, CR, BNB, SP, SF refer to metamorphic basement, Burcei, Monte Cresia, Monte Nai, Cala Regina, Brunco Nicola Bove, San Priamo, Sette Fratelli units, respectively. SO refers to synplutonic mafic masses of Cala Regina Unit.

granodiorites areal distribution, depicting a sharp difference between a much more radiogenic northern part of the pluton, dominated by leucogranites, and a less radiogenic southern part, in which granodioritic rock-units prevail. Likewise, the more radiogenic nature of the granodioritic/monzogranitic Monte Nai Unit allows to discriminate it with respect to the granodioritic Cala Regina and Monte Cresia Units, while the peraluminous satellite intrusions of the Monte Maria Unit emerge as higher radiogenic spots within the southern low radiogenic part of the pluton.

3.3. Petrography and geochronology

Main petrographic features of Sàrrabus igneous units are outlined in Conte, Cuccuru, et al. (2018), Conte et al. (2017), Conte, Naitza, et al. (2018) and summarized in Figure 7 and Table 2. Overall textural and mineralogical features, as well as chemical signatures, confirm the discrimination of different intrusive units recognized in the field and was used to support mapping.

Petrographic differences observed in the granodioritic rock-units regard mainly the increasing (a) size and content of dark enclaves (from tonalitic to

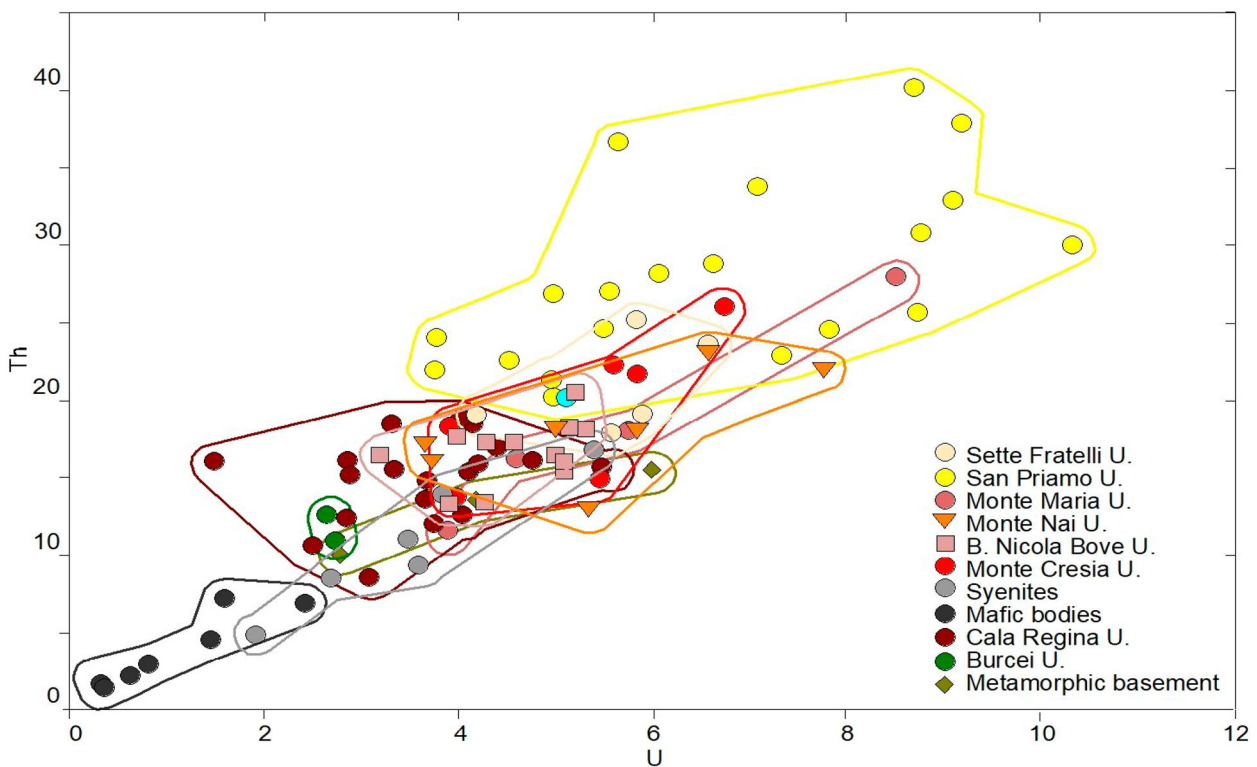


Figure 5. U/Th plot for mapped intrusive units and surrounding metamorphic rocks basement. U and Th contents are expressed in ppm.

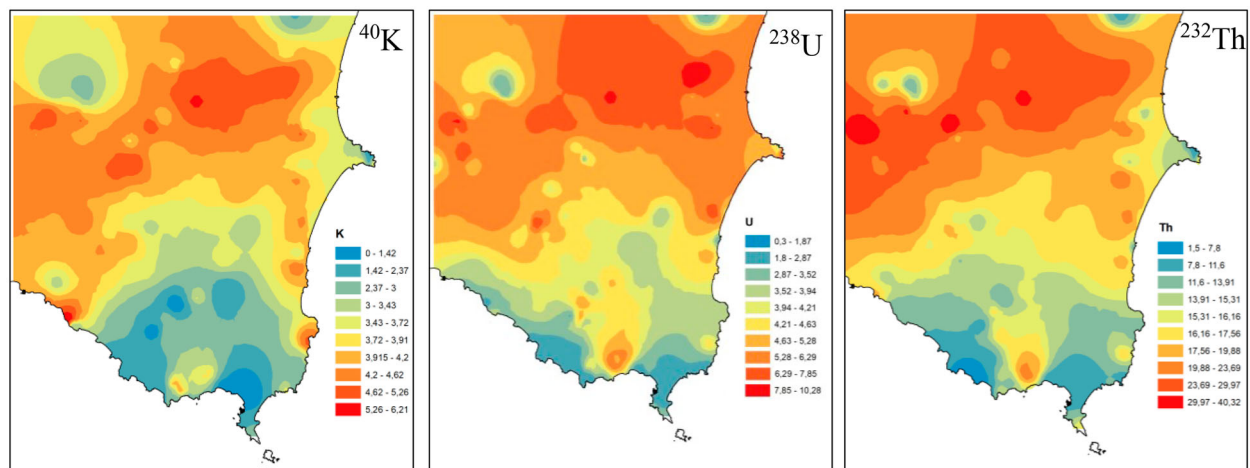


Figure 6. ^{40}K , ^{238}U and ^{232}Th density maps for Sàrrabus igneous units.

hornblende quartz gabbros), (b) color index (from 14% to 20%), as well as (c) incidence of primary hornblende (1%–4%) from Monte Cresia and Monte Nai Units to Cala Regina Unit, respectively. Plagioclase with relic calcic cores commonly observed in granodioritic rocks are locally documented in Monte Nai granodiorites (Figure 6(a)).

Conversely, a wide range of petrographic variations is observed for felsic rock-types in terms of mafic mineralogy, feldspar composition and accessory phases (Figures 6(b–d)). Brunco Nicola Bove Unit ranges from biotite monzogranite to leucogranite; these rock-types are characterized by a normal oligoalbitic plagioclase (An_{30-15}). The San Priamo Unit is made up of biotite leucogranite showing a more calcic plagioclase (An_{40-26} ; Conte et al., 2017) and large allanite grains as typical accessory mineral. The Monte Maria Unit granites are garnet-bearing two-mica varieties, whereas the Monte Sette Fratelli Unit is characterized by the unusual early Fe-hastingsitic amphibole, as well as by annitic dark mica, fluorite and fayalite as late-stage phases (Conte et al., 2017; Secchi & Lorrain, 2001).

Mafic intrusions and mafic dikes show similar petrographic fingerprints (Figures 7(e,f)). According to Brotzu et al. (1993), Burcèi Unit ranges from mesocratic gabbroic rocks to tonalites characterized by the common occurrence of ortho- and clinopyroxene, reddish biotite and only ilmenite as Fe-oxide phase (Figure 7(g)). Conversely, dismembered mafic masses in Cala Regina Unit (SO complex) are hornblende gabbroic rocks with relics of orthopyroxene followed by clinopyroxene, grading to hornblende quartz gabbros. The SO complex also comprises olivine-bearing gabbroic rocks and leuco-gabbros with cumulate textures (Conte, Cucuru, et al., 2018; Secchi & Lorrain, 2001). Remarkably, an orthopyroxene \rightarrow clinopyroxene succession replaced by amphibole, is also frequently observed in the spessartitic mafic dikes.

Epysienitic rocks (S) along the SSSZ range from (a) spotted rocks, consisting of variably albitized plagioclase with anhedral K-feldspar, aggregates of low-Ti diopside partly to totally replaced by hastingsite amphibole (Figure 7(h)) and (b) deeply metasomatized rocks with xenomorphic or granoblastic textures containing andraditic garnet and Na-rich diopside. In quartz-bearing varieties, cataclastic microtextures (e.g. mortar and/or granoblastic textures) are frequently observed (Pirinu et al., 1996).

Geochronological data obtained with different systematics indicate coherent ages. New U/Pb zircon dating of the Cala Regina Unit granodiorite sampled in Capo Carbonara yield an age of 286 ± 9 Ma (Figure 8(a)), which is undistinguishable from a Rb/Sr isochron obtained from selected Cala Regina Unit granodiorite samples, which yield an age of 292 ± 17 Ma (Figure 8(b)). Remarkably, the obtained values are undistinguishable from those found by Nicoletti et al. (1982) by two conventional K/Ar internal isochrons for granodiorites from Capo Carbonara, which gave ages of 285 ± 11 and 286 ± 5 Ma.

More regional constraints are provided by the Rb/Sr geochronological data reported in Ronca et al. (1999) for garnet-bearing peraluminous dikes, giving ages in the range of $281\text{--}293 \pm 3$ Ma. Based on the whole available data set, the U/Pb value assume the role of emplacement age of the entire pluton.

In this reconstruction, the Burcèi Unit belongs to an earlier ilmenite rock-series predating the growth of Sàrrabus igneous massif, also recognized in the Arbus igneous complex of southern Sardinia (Secchi et al., 1991). Besides the compositional affinities, a further constrain in favor of a single early mafic event framed into the OMP of southern Sardinia (Conte et al., 2017), is provided by the Rb/Sr age of 311 ± 9 Ma obtained for Burcèi gabbrotonalites (Brotzu et al., 1993), which is undistinguishable, inside the correlated error, from the age of Arbus intrusives

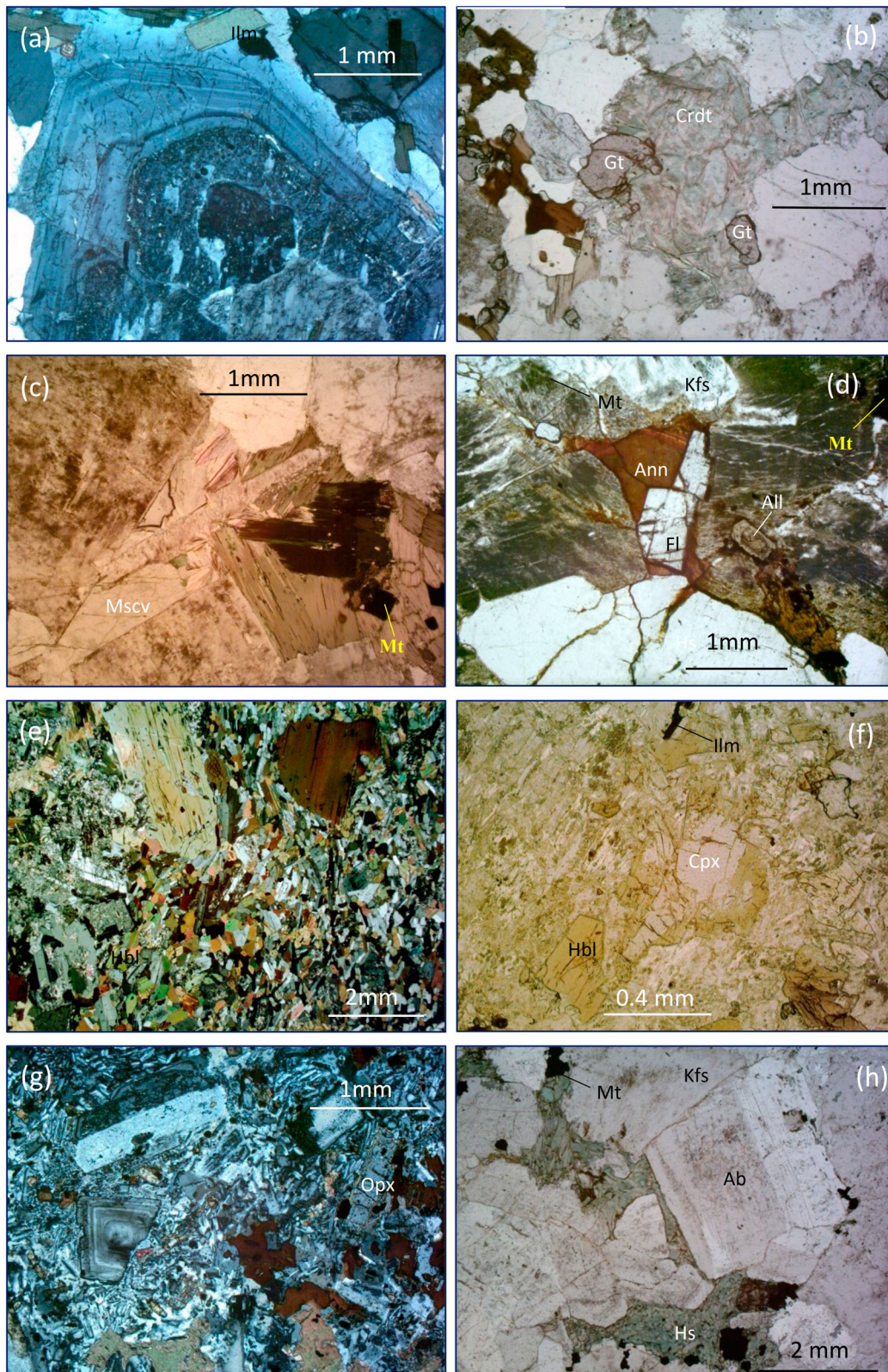


Figure 7. Petrographic characters of representative magmatic rocks from Sàrrabus pluton. (a) Large patchy-zoned plagioclase lath with relic calcic core on Monte Nai Unit granodiorite (crossed polars; sample ESP1, Monte Nai) (b) garnet associated to pinitized cordierite in Monte Maria peraluminous granite (plane polarized light; sample LPC, Scala Carbonara); (c) interstitial white mica related to incipient greisening processes in San Priamo Unit leucogranite (plane polarized light; sample SPP9, Monte Gruttas); (d) interstitial fluorite and annite in leucogranite of Monte Sette Fratelli Unit (plane polarized light; sample GP11, Baccu Malu); (e) panidiomorphic textures of quartz microgabbro in SO complex of Cala Regina Unit (crossed polars; sample SSP17; Capo Carbonara); (f) Clinopyroxene/brown amphibole relationships on equigranular varieties of spessartitic dike, (crossed polars; sample ESP10; Olia Speciosa); (g) porphyritic texture and graphic groundmasses of gabbrotonalite from Burcèi Unit (crossed polars sample BG17, Burcèi); (h) example of automorphic texture of epsyenite associated to Cala Regina Unit granodiorites (plane polarized light; sample SSP14a, Marroccu). Abbreviations as in Table 2.

for which a U/Pb value of 304 ± 1 Ma is reported (Cuccuru et al., 2016).

3.4. Structural field evidence

The Sàrrabus pluton emplaced in lower Cambrian to Silurian anchimetamorphic metasediments at very shallow crustal levels in the frontal part of Variscan Nappe Zone (Carmignani et al., 1994) of the Sardinian basement. Shallow crustal emplacement (about 6 km) is constrained by: (1) the occurrence of a narrow (less than 200 m wide) andalusite-cordierite-dark mica aureole in the host basement along with the intrusive contact; (2) the Al-in hornblende barometer, which yields values close to 2 kb in the Cala Regina granodiorite, and up to 1 kb in the Monte Sette Fratelli granite (Conte, Cuccuru, et al., 2018; Conte et al., 2017; Conte, Naitza, et al., 2018). The contacts with the country rocks are widely exposed along to the northern boundary of the pluton; small remnants of the basement rocks locally occur along the Southern coastline (Geremeas) and may testify a possible southern closure of the pluton.

Different emplacement trends characterize the different units: three units, Monte Cresia S. Priamo and Bruncu Nicola Bove show reciprocal intrusive contacts parallel to the contact between the older intrusion (i.e. the Monte Cresia granodiorite) and the anchimetamorphic Palaeozoic metasediments.

A switch towards EW direction characterizes the steep contact between Cala Regina and Bruncu Nicola Bove units. The Cala Regina granodiorite in its central part exhibits a marked planar anisotropy defined by dark enclaves and dark micas. Along the southern coastline, this foliation abruptly steepens along an EW trending belt strongly enriched in mafic-intermediate – in place highly stretched – microgranular enclaves (Figure 2(c)), synplutonic mafic blobs of different size, stretched at different degrees, which are encircled by elliptical to ribbon-like –straight to convolute – (Figure 2(b)) mafic dispersions. These features are suggestive of a shear enhanced mingling between different magmas as commonly occurs in calcalkaline plutons (Barbarin & Didier, 1992; Valle Aguado et al., 2017; Zorpi et al., 1991).

The association of mingled mafic rocks and highly strained mafic enclaves along a 2 km-wide belt are evidence for an important EW trending synplutonic shear zone; hereafter South Sarrabus Shear zone (SSSZ). This shear belt hosts episyenite bodies, which displays deformational microtextures such as quartz subgrains (Pirinu et al., 1996), and ectometric slices of monzogranitic granodiorites with strongly foliated fabrics suggestive of sub-magmatic to solid state flow. The long axis of the stretched enclaves and the lineations defined by the K-feldspar megacrysts in the monzogranitic granodiorite

systematically plunge down deep (Figure 2(d)). These features are suggestive of a vertical flow along a dilatant shear zone where the Cala Regina granodiorite is possibly rooted at depth as a product of mixing processes sustained by a thermal input able to lower the viscosity contrast between felsic and mafic magmas (Georgiev et al., 2009; Prabhakar et al., 2009). At shallow levels, the temperature lowering resulted in mingling and localized hybridization generating tonalitic sheets. The intrusion inflation exceeding the dilation rate was mainly accommodated by upwards and lateral emplacement at upper crustal levels within a fractured crust. This accounts for flat foliation away from SSSZ. The occurrence of repeated, variably mingled, mafic injections observed Cala Regina Unit, indicates that the SSSZ acted as the feeder of this unit.

Changes in stress coordinates, are constrained during the complete cooling and partially uplifted igneous massif (Martinez-Poza and Druguet, 2016), which control the late emplacement of shallower peraluminous intrusions (i.e. Monte Maria Unit) and the later bimodal dike swarm.

4. Ore deposits

In the mapped region, granite-related ore deposits and occurrences are hosted in low-grade metamorphics of the Variscan basement and, in minor amount, in the northernmost intrusive units of Sàrrabus igneous massif. They may be grouped (Funedda et al., 2018; Naitza et al., 2015) as: (a) Zn–Cu–Pb sulfide skarns and (b) F–Ba ± Pb–Ag–Cu–Zn vein systems. Only the (b)-type ores are reported in the map and here examined, as they appear closely involved with the petrogenetic processes of the granitoid suites of the Sàrrabus massif (Conte et al., 2017). The fluorite-barite ± Pb–Ag–Cu–Zn sulfide hydrothermal vein systems develop along the EW and NNW structural patterns (Valera, 1974). EW silver-rich polymetallic veins form a narrow swarm (the so-called ‘Sàrrabus silver lode’) that runs alongside the northern borders of the igneous massif, up to 4 km from intrusive contact; they mainly follow major fault lineaments in the basement and locally crosscut the Monte Cresia Unit granodiorites. The NNW trending sulfide-poor and fluorite-barite rich veins widely occur outside the northern edge of the pluton (Valera, 1974), but a noticeable cluster is recognized in the western part of the area, forming a mineralized NW belt that runs for over 4 km from the Sette Fratelli Unit intrusion to the Monte Genis granite and, still further, towards the Silius mine district, which represents one of the largest fluorite vein deposit in Europe. The close-field association and the geochemical affinity of the ores with the fluorite-bearing granites that form the northern part of the Sàrrabus igneous massif (i.e.

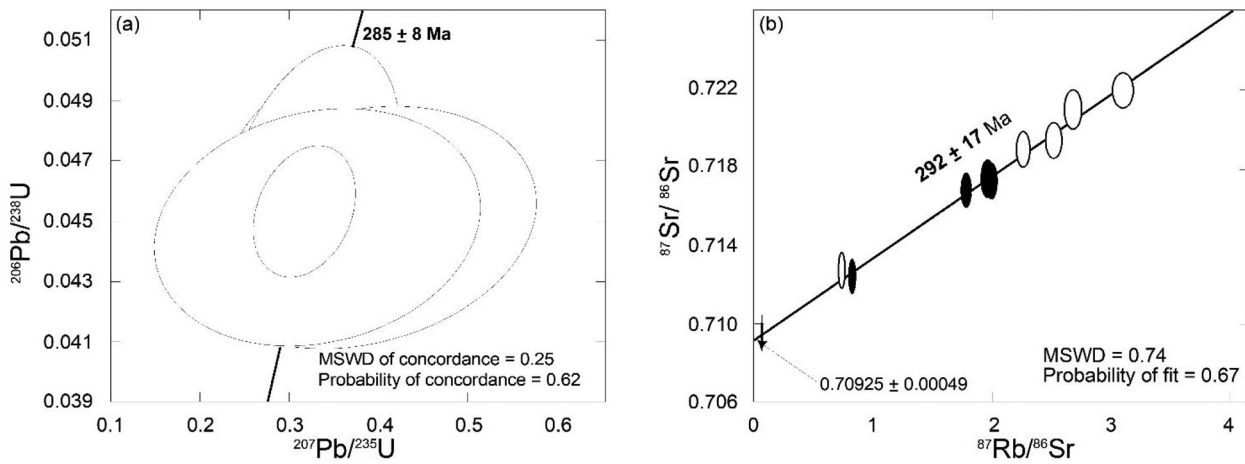


Figure 8. Geochronological data for Sàrrabus granodiorites. (a) U/Pb concordia diagram for zircons of SSP2 sample (Capo Carbonara) and (b) Rb/Sr regression line of whole-rock (including a plagioclase concentrate close to the $^{87}\text{Sr}/^{86}\text{Sr}$ intercept) selected samples of Cala Regina granodiorite. Solid symbols refer to data after Nicoletti et al. (1982) and Poli and Tommasini (1999); open symbols after Conte, Naitza, et al. (2018). Plotted data include 2σ decay constant errors.

San Priamo and Monte Sette Fratelli Units) clearly indicate a genetic linkage (Castorina et al., 2020; Conte et al., 2017). The whole southern sector of the Sàrrabus pluton is virtually devoid of ore mineralization, as expected by the lack of F-bearing granites (Main Map).

5. Conclusions

The exposed geological map at 1:50,000 scale portrays a circumscribed multiple and composite Variscan pluton, characterized by a decreasing interaction between mafic and felsic magmas, resulting in the emplacement of several intrusive units at shallow crustal levels. The whole data set is consistent with fast growth of the pluton during the granodioritic stage (i.e. Monte Cresia, Monte Nai and Cala Regina Units). In this stage,

granodiorites are generated either as magmas of possible lower crustal anatectic origin (Monte Cresia, Monte Nai) and as magma related to mantle/crustal interaction (Cala Regina Unit), suggesting a zoned reservoir at depth. After the emplacement of the Cala Regina unit, the felsic activity increases, as testified by Bruncu Nicola Bove and S.Priamo granites (Figure 9). The growth stage ended with a voluminous mafic and felsic activity represented by swarms of NNW dikes, whose frequency and thickness are higher in the Cala Regina Unit. F-bearing granites, such as Monte Sette Fratelli unit, seal up the – N70 trending – contact between Monte e Cresia and S.Priamo units. These intrusives represent the late stage of the pluton growth. The major hydrothermal vein systems and ore deposits of the region may be related to this late stage.

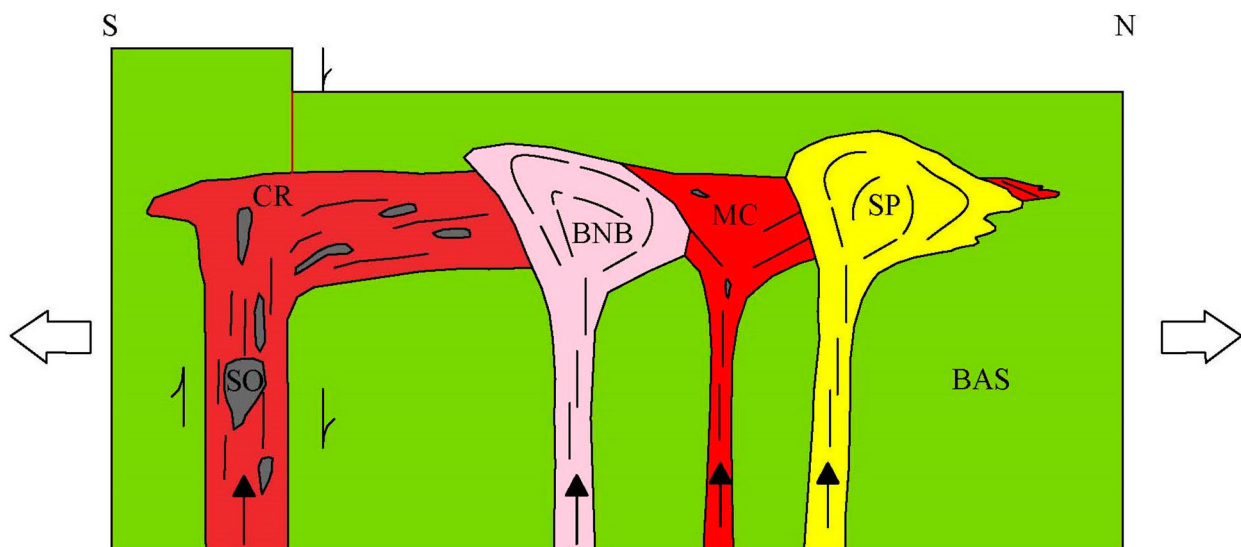


Figure 9. Schematic emplacement model for Sàrrabus pluton (not to scale). BAS, MC, CR, BNB ad SP refer to metamorphic basement, Monte Cresia, Cala Regina, Bruncu Nicola Bove, San Priamo units, respectively. SO refers to synplutonic mafic masses of Cala Regina Unit.

Ascribing the sequential growth of the Sàrrabus granitic massif to a well-defined mechanism, in the lack of well-exposed boundaries with the host Variscan basement, should be largely hypothetical. Nevertheless, considering that in the early Permian the crustal sector of Sardinia was involved in the intra-Pangea megashear system during its early Permian rotation (Aubele et al., 2014; Edel et al., 2014), several mechanisms related to this strike slip dynamic can account for the generation of dilational zones bounded by normal fault and normal shears. Among these, the emplacement at dilational step over (El Desouky et al., 1996) or at termination of strike slip faults (Valle Aguado et al., 2017) are compatible with the late Carboniferous-early Permian wrench faults network (e.g. the dextral NS trending Quirra Fault) that affects the Sardinian Variscan Basement.

Software

Overlaying of maps, geostatistical interpolations and digitalization of the final maps were carried out using Esri Arc GIS 9. Field spectrometric analysis was performed using jRadview. The isotopic composition of monazite grains was analyzed using the Glitter package.

U/Pb concordia diagrams (2σ error ellipses), concordia ages (95% confidence level), and Rb/Sr data were processed using Isoplot 4.1 computer program (Ludwig, 2012).

Acknowledgements

This work was supported by RAS L.R. 7/2007 research program ‘Il blocco SardoCorso: area chiave per la ricostruzione della geodinamica varisica’ CUP J81G17000110002 and by RAS/FdS research program ‘Geogenic and anthropogenic sources of minerals and elements: fate and persistency over space and time in sediments’ CUP F74I19000960007. The authors are indebted with the Editors and Heike Apps, Giovanni Musumeci, Lucy Sant’Anna and an anonymous cartographer, whose reviews and useful suggestions greatly improved the paper. Special thanks to FO.RE.S.-T.A.S. for the access to the natural reserve of Monte Sette Fratelli and to Alessandro Grosso and Daniele De Lisa for part of the graphic work.

Disclosure statement

No potential conflict of interest was reported by the author(s).


Funding

This work was supported by Fondazione di Sardegna [grant number CUP F74I19000960007]; Regione Autonoma della Sardegna [grant number CUP J81G17000110002].

Data availability statement

The data that support the findings of this study are available from the corresponding author [SN], upon reasonable request.

ORCID

F. Secchi  <http://orcid.org/0000-0002-7340-1011>
 S. Naitza  <http://orcid.org/0000-0003-4125-9222>
 G. Oggiano  <http://orcid.org/0000-0003-1236-1498>
 S. Cuccuru  <http://orcid.org/0000-0002-0175-3616>

References

- Aubele, K., Bachtadse, V., Muttoni, G., & Ronchi, A. (2014). Paleomagnetic data from late paleozoic dykes of sardinia: Evidence for block rotations and implications for the intra-Pangea megashear system. *Geochemistry, Geophysics, Geosystems*, 15(5), 1684–1697. <https://doi.org/10.1002/2014GC005325>
- Barbarin, B., & Didier, J. (1992). Genesis and evolution of mafic microgranular enclaves through various types of interaction between coexisting felsic and mafic magmas. *Earth and Environmental Science Transactions of The Royal Society of Edinburgh*, 83(1-2), 145–153. <https://doi.org/10.1017/S0263593300007835>
- Bonin, B. (2004). Do coeval mafic and felsic magmas in post-collisional to within-plate regimes necessarily imply two contrasting, mantle and crustal, sources? A review. *Lithos*, 78(1-2), 1–24. <https://doi.org/10.1016/j.lithos.2004.04.042>
- Bralia, A., Ghezzi, C., Guasparri, G., & Sabatini, G. (1982). Aspetti genetici del batolite sardo-corso. *Rendiconti Società Italiana di Mineralogia e Petrografia*, 38(2), 701–764.
- Brotzu, P., Callegari, E., & Secchi, F. (1993). The search for the parental magma of the high-K calc-alkaline igneous rocks series in the southernmost Sardinia batholith. *Periodico di Mineralogia*, 63, 253–280.
- Cacioli, A., Baldoncini, M., Bezzon, G. P., Broggin, C., Buso, G. P., Callegari, I., Colonna, T., Fiorentini, G., Guastaldi, E., Mantovani, F., Massa, G., Menegazzo, R., Mou, L., Rossi, A. C., Shyti, M., Zanon, A., & Xhixha, G. (2012). A new FSA approach for in situ γ ray spectroscopy. *Science of the Total Environment*, 414, 639–645. <https://doi.org/10.1016/j.scitotenv.2011.10.071>
- Carmignani, L., Carosi, R., Di Pisa, A., Gattiglio, M., Musumeci, G., Oggiano, G., & Pertusati, P. C. (1994). The Hercynian chain in Sardinia (Italy). *Geodinamica Acta*, 7(1), 31–47. <https://doi.org/10.1080/09853111.1994.11105257>
- Casini, L., Cuccuru, S., Maino, M., Oggiano, G., Puccini, A., & Rossi, P. (2015). Structural map of Variscan northern Sardinia (Italy). *Journal of Maps*, 11(1), 75–84. <https://doi.org/10.1080/17445647.2014.936914>
- Casini, L., Cuccuru, S., Maino, M., Oggiano, G., & Tiepolo, M. (2012). Emplacement of the arzachena pluton (Corsica-Sardinia batholith) and the geodynamics of the incoming pangea. *Tectonophysics*, 544–545, 31–49. <https://doi.org/10.1016/j.tecto.2012.03.028>
- Casini, L., Cuccuru, S., Puccini, A., Oggiano, G., & Rossi, P. (2015). Evolution of the corsica–Sardinia batholith and late-orogenic shearing of the variscides. *Tectonophysics*, 646, 65–78. <https://doi.org/10.1016/j.tecto.2015.01.017>

- Castorina, F., Masi, U., & Gorello, I. (2020). Rare earth element and Sr-Nd isotopic evidence for the origin of fluorite from the Silius vein deposit (southeastern sardinia, Italy). *Journal of Geochemical Exploration*, 215, 106535. <https://doi.org/10.1016/j.gexplo.2020.106535>
- Cocherie, A., Rossi, P., Fanning, C. M., & Guerrot, C. (2005). Comparative use of TIMS and SHRIMP for U–Pb zircon dating of A-type granites and mafic tholeiitic layered complexes and dykes from the corsican batholith (France). *Lithos*, 82(1-2), 185–219. <https://doi.org/10.1016/j.lithos.2004.12.016>
- Cocherie, A., Rossi, P., Fouillac, A. M., & Vidal, P. (1994). Crust and mantle contributions to granite genesis - an example from the Variscan batholith of corsica, France, studied by trace element and Nd-Sr-O-isotope systematics. *Chemical Geology*, 115(3-4), 173–211. [https://doi.org/10.1016/0009-2541\(94\)90186-4](https://doi.org/10.1016/0009-2541(94)90186-4)
- Conte, A. M., Cuccuru, S., D'Antonio, M., Naitza, S., Oggiano, G., & Secchi, F. (2018). Long-lasting mantle-derived activity and evolution in the late-Variscan Sàrrabus igneous complex (SE Sardinia, Italy). *Abstract Book Congresso Congiunto SIMP-SGI, Catania, 12-14 Settembre 2018*, <https://doi.org/10.3301/ABSGI/2018.02>
- Conte, A. M., Cuccuru, S., D'Antonio, M., Naitza, S., Oggiano, G., Secchi, F., Casi, L., & Cifelli, F. (2017). The post-collisional late Variscan ferroan granites of southern Sardinia (Italy): inferences for inhomogeneity of lower crust. *Lithos*, 294–295, 263–282. <https://doi.org/10.1016/j.lithos.2017.09.028>
- Conte, A. M., Naitza, S., Oggiano, G., Secchi, F., Cuccuru, S., Casini, L., & Puccini, A. (2018). Architecture, emplacement mode of late-Variscan plutons and their relationships with post-collisional phases: Examples from Sarrabus igneous massif (SE Sardinia, Italy). *Abstract Book Congresso Congiunto SIMP-SGI, Catania, 12-14 Settembre 2018*, <https://doi.org/10.3301/ABSGI/2018.02>
- Cruciani, G., Franceschelli, M., Groppo, C., Oggiano, G., & Spano, M. E. (2015). Re-equilibration history and P–T path of eclogites from Variscan Sardinia, Italy: A case study from the medium-grade metamorphic complex. *International Journal of Earth Sciences*, 104(3), 797–814. <https://doi.org/10.1007/s00531-014-1095-5>
- Cruciani, G., Franceschelli, M., Musumeci, G., & Scodina, M. (2020). Geology of the montigu nieddu metamorphic basement, NE Sardinia (Italy). *Journal of Maps*, 16(2), 543–551. <https://doi.org/10.1080/17445647.2020.1785344>
- Cuccuru, S., Casini, L., Oggiano, G., & Simula, E. N. (2018). Structure of the castellaccio pluton (asinara island, Italy). *Journal of Maps*, 14(2), 293–302. <https://doi.org/10.1080/17445647.2018.1463297>
- Cuccuru, S., Naitza, S., Secchi, F., Puccini, A., Casini, L., Pavanetto, P., Linnemann, U., Hofmann, M., & Oggiano, G. (2016). Structural and metallogenic map of late Variscan Arbus pluton (SW Sardinia, Italy). *Journal of Maps*, 12(5), 860–865. <https://doi.org/10.1080/17445647.2015.1091750>
- Di Vincenzo, G., Andriessen, P. A., & Ghezzi, C. (1996). Evidence of Two different components in a Hercynian peraluminous cordierite bearing granite: The San basilio intrusion (central Sardinia, Italy). *Journal of Petrology*, 37(5), 1175–1206. <https://doi.org/10.1093/petrology/37.5.1175>
- Edel, J. B., Casini, L., Oggiano, G., Rossi, P., & Schulmann, K. (2014). Early Permian 90° clockwise rotation of the maures–esterel–corsica–Sardinia block confirmed by new palaeomagnetic data and followed by a triassic 60° clockwise rotation. *Geological Society London Special Publications*, 405(1), 333–361. <https://doi.org/10.1144/SP405.10>
- El Desouky, M., Feely, M., & Mohr, P. (1996). Diorite-granite magma mingling and mixing along the axis of the galway granite batholith, Ireland. *Journal of the Geological Society. London*, 153(1996), 361–374. <https://doi.org/10.1144/gsjgs.153.3.0361>
- Ferré, E. C., & Leake, B. E. (2001). Geodynamic significance of early orogenic high-K crustal and mantle melts: Example of the Corsica batholith. *Lithos*, 59(1-2), 47–67. [https://doi.org/10.1016/s0024-4937\(01\)00060-3](https://doi.org/10.1016/s0024-4937(01)00060-3)
- Frost, B. R., Barnes, C. G., Collins, W. J., Arculus, R. J., Ellis, D. J., & Frost, C. D. (2001). A geochemical classification for granitic rocks. *Journal of Petrology*, 42, 2033–2048.
- Frost, C. D., & Frost, B. R. (2011). On ferroan (A-type) granitoids: Their compositional variability and modes of origin. *Journal of Petrology*, 52(1), 39–53. <https://doi.org/10.1093/petrology/egq070>
- Funedda, A., Naitza, S., Butta, C., Cocco, F., & Dini, A. (2018). Structural controls of ore mineralization in a polydeformed basement: Field examples from the Variscan Baccu locci shear zone (SE Sardinia, Italy). *Minerals*, 8(10), 456. <https://doi.org/10.3390/min8100456>
- Georgiev, N., Henry, B., Jordanova, N., Froitzheim, N., Jordanova, D., Ivanov, I., & Dimov, D. (2009). The emplacement mode of upper cretaceous plutons from the southwestern part of the sredna gora zone (Bulgaria): structural and AMS study. *Geologica Carpathica*, 60(1), 15–33. <https://doi.org/10.2478/v10096-009-0001-8>
- Giovanardi, T., Mazzucchelli, M., Lugli, F., Girardi, V. A. V., Correia, C. T., Tassinari, C. C. G., & Cipriani, A. (2018). Isotopic constraints on contamination processes in the tonian goiás stratiform complex. *Lithos*, 310–311, 136–152. <https://doi.org/10.1016/j.lithos.2018.04.008>
- Kaçeli Xhixha, A. M., Albèri, M., Baldoncini, M., Bezzon, G. P., Buso, G. P., Callegari, I., Casini, L., Cuccuru, S., Fiorentini, G., Guastaldi, E., Mantovani, F., Mou, L., Oggiano, G., Puccini, A., Rossi, A. C., Strati, V., Xhixha, G., & Zanon, A. (2016). Uranium distribution in the Variscan basement of northeastern sardinia. *Journal of Maps*, 12(5), 1029–1036. <https://doi.org/10.1080/17445647.2015.1115784>
- Kretz, R. (1983). Symbols for rock-forming minerals. *American Mineralogist*, 68, 277–279.
- Ludwig, K. R. (2012). Isoplot 3.75. A geochronological toolkit for microsoft excel. *Berkeley Geochronology Center. Special Publication*, 5.
- Martinez-Poza, A. I., & Druguet, E. (2016). Structure and tectonic setting of the SE Sardinia mafic dyke swarm. Insights for the stress state during magma emplacement in the upper crust. *Journal of Geodynamics*, 101, 170–185. <https://doi.org/10.1016/j.jog.2016.05.012>
- Matte, P. (1986). Tectonics and plate tectonic model for the varican belt of Europe. *Tectonophysics*, 126(2-4), 329–274. [https://doi.org/10.1016/0040-1951\(86\)90237-4](https://doi.org/10.1016/0040-1951(86)90237-4)
- Naitza, S., Oggiano, G., Casini, L., Cuccuru, S., Secchi, F., Funedda, A., & Tocco, S. (2015). Structural and magmatic controls on late Variscan metallogenesis: Evidences from southern Sardinia (Italy). *13th Biennial SGA Meeting, Nancy, France, Proceedings, volume 1*, 161–164.
- Nicoletti, M., Ardanese, L. R., & Colasanti, S. (1982). La granodiorite di Capo Carbonara (sardegna-italia). Età K-Ar di fasi minerali in paragenesi. *Rendiconti Società Italiana di Mineralogia e Petrologia*, 38(2), 765–769.
- Paquette, J. L., Ménot, R.-P., Pin, C., & Orsini, J. B. (2003). Episodic and short-lived granitic pulses in a post-

- collisional setting: Evidence from precise U–Pb zircon dating through a crustal cross-section in Corsica. *Chemical Geology*, 198(1–2), 1–20. [https://doi.org/10.1016/S0009-2541\(02\)00401-1](https://doi.org/10.1016/S0009-2541(02)00401-1)
- Pirinu, N., Brotzu, P., Callegari, E., & Secchi, F. (1996). Age and field relationships of albite-rich monzosyenites intruded into late-Hercynian granitoids of Sàrrabus area (SE Sardinia, Italy). *Periodico di Mineralogia*, 65, 289–304.
- Poli, G., Ghezzi, C., & Conticelli, S. (1989). Geochemistry of granitic rocks from the Hercynian Sardinia-Corsica batholith: Implication for magma genesis. *Lithos*, 23(4), 247–266. [https://doi.org/10.1016/0024-4937\(89\)90038-8](https://doi.org/10.1016/0024-4937(89)90038-8)
- Poli, G., & Tommasini, S. (1999). Geochemical modelling of acid-basic magma interaction in the Sardinia-Corsica batholith: The case study of Sàrrabus, southeastern Sardinia, Italy. *Lithos*, 46(3), 553–571. [https://doi.org/10.1016/S0024-4937\(98\)00082-6](https://doi.org/10.1016/S0024-4937(98)00082-6)
- Prabhakar, B. C., Jayananda, M., Shareef, M., & Kano, T. (2009). Synplutonic mafic injections into crystallizing granite pluton from Gurgunta area, northern part of eastern Dharwar craton: Implications for magma chamber processes. *Journal Geological Society of India*, 74(2), 171–188. <https://doi.org/10.1007/s12594-009-0120-y>
- Puccini, A., Xhixha, G., Cuccuru, S., Oggiano, G., Xhixha, M. K., Mantovani, F., & Casini, L. (2014). Radiological characterization of granitoid outcrops and dimension stones of the Variscan Corsica-Sardinia batholith. *Environmental Earth Sciences*, 71(1), 393–405. <https://doi.org/10.1007/s12665-013-2442-8>
- Regione Autonoma Sardegna. (2005). *Ikonos 2005 satellite imagery*. https://webgis2.regione.sardegna.it/catalogo-dati/card.jsp?uuiid=R_SARDEG:DYYBK
- Ronca, S., Del Moro, A., & Traversa, G. (1999). Geochronology, Sr–Nd isotope geochemistry and petrology of late Hercynian dike magmatism from Sàrrabus (SE Sardinia). *Periodico di Mineralogia*, 68, 231–260.
- Rossi, P., & Cocherie, A. (1991). Genesis of a Variscan batholith: Field, petrological and mineralogical evidence from the Corsica-Sardinia batholith. *Tectonophysics*, 195(2–4), 319–346. [https://doi.org/10.1016/0040-1951\(91\)90219-I](https://doi.org/10.1016/0040-1951(91)90219-I)
- Rossi, P., Cocherie, A., & Fanning, C. M. (2015). Evidence in Variscan Corsica of a brief and voluminous late Carboniferous to early Permian volcanic-plutonic event contemporaneous with a high-temperature/low-pressure metamorphic peak in the lower crust. *Bulletin de la Société Géologique de France*, 186(2–3), 171–192. <https://doi.org/10.2113/gssgfbull.186.2-3.171>
- Rossi, P., Oggiano, G., & Cocherie, A. (2009). A restored section of the “southern Variscan realm” across the Corsica–Sardinia microcontinent. *Comptes Rendus Geoscience*, 341(2–3), 224–238. <https://doi.org/10.1016/j.crte.2008.12.005>
- Secchi, F., Brotzu, P., & Callegari, E. (1991). The Arburese igneous complex: An example of igneous fractionation leading to peraluminous granites as residual melts. *Chemical Geology*, 92(1–3), 213–249. [https://doi.org/10.1016/0009-2541\(91\)90057-X](https://doi.org/10.1016/0009-2541(91)90057-X)
- Secchi, F., & Lorrain, M. (2001). Some geological and environmental aspects of the Sàrrabus-gerrei region (SE Sardinia, Italy). *Rendiconti Seminari Facoltà di Scienze Università di Cagliari Supplemento*, 71, 187–208.
- Tommasini, S., Poli, G., & Halliday, A. N. (1995). The role of sediment subduction and crustal growth in Hercynian plutonism: Isotopic and trace element evidence from the Sardinia-Corsica Batholith. *Journal of Petrology*, 36(5), 1305–1332. <https://doi.org/10.1093/petrology/36.5.1305>
- Valera, R. (1974). Genesi ed evoluzione delle mineralizzazioni del Sàrrabus (Sardegna sud-orientale). *Rendiconti Società Italiana di Mineralogia e Petrologia*, 30, 1081–1108.
- Valle Aguado, B., Azevedo, M. R., Nolan, J., Medina, J., Costa, M. M., Corfu, F., & Martínez Catalán, J. R. (2017). Granite emplacement at the termination of a major Variscan transcurrent shear zone: The late collisional Viséu batholith. *Journal of Structural Geology*, 98, 15–37. <https://doi.org/10.1016/j.jsg.2017.04.002>
- Virdis, S. G. P., Oggiano, G., & Disperati, L. (2012). A geomatics approach to multitemporal shoreline analysis in western Mediterranean: The case of Platamona-Maritza beach (northwest Sardinia, Italy). *Journal of Coastal Research*, 28(3), 624–640. <https://doi.org/10.2112/JCOASTRES-D-11-00078.1>
- Whitney, D. L., & Evans, B. W. (2010). Abbreviations for names of rock-forming minerals. *Amer. Mineral*, 95(1), 185–187. <https://doi.org/10.2138/am.2010.3371>
- Zorpi, M. J., Coulon, C., & Orsini, J. B. (1991). Hybridization between felsic and mafic magmas in calcalkaline granitoids: A case study in northern Sardinia, Italy. *Chemical Geology*, 92(1–3), 45–86. [https://doi.org/10.1016/0009-2541\(91\)90049-W](https://doi.org/10.1016/0009-2541(91)90049-W)